Progress In Electromagnetics Research B, Vol. 36, 173–191, 2012

A HIERARCHICAL TREE SHAPED POWER DISTRIBUTION NETWORK BASED ON CONSTRUCTAL THEORY FOR EBG STRUCTURE POWER PLANE

H.-F. Huang, S.-Y. Liu*, and W. Guo

School of Electronic and Information Engineering, South China University of Technology, Guangzhou 510640, China

Abstract—In this paper, a tree-shaped power distribution network is designed based on constructal theory for planar EBG structure power plane on PCB, in order to optimize DC performance. Planar EBG structures suppress noise, and the network provides currents to them. This network is composed of hierarchical metal paths. The geometric parameters can be optimized based on the concept of constructal theory. The optimal performance consists of constructing the given area in a sequence of building blocks from the smallest size toward larger sizes hierarchically. In the meantime, a PCB power plane is developed with 2nd order tree-shaped constructal network. Analysis illustrates that EBG power plane with constructal tree shaped network has multifunctions of low voltage drop, current equidistribution and effective noise isolation.

1. INTRODUCTION

Increasing higher frequencies and decreasing voltage levels result in signal integrity and power integrity problems at any of the chip, package, and board levels. The simultaneous switching noise (SSN) can propagate between the power planes and affect the whole system [1, 2]. SSN is recognized as one of the most significant issues in modern high speed digital systems design. Recently, various planar electromagnetic band-gap (EBG) structures have been proposed and applied in power/ground plane pairs to mitigate SSN [2–12]. They consist of two metallic layers of the multilayer PCB, one of which is solid (ground plane) and the other a patterned one (power plane). This patterned plane consists of array of unit cells [2]. The unit cells of EBG structure

Received 10 August 2011, Accepted 28 October 2011, Scheduled 10 November 2011
* Corresponding author: Shiyun Liu (shiyunliu1986@gmail.com).

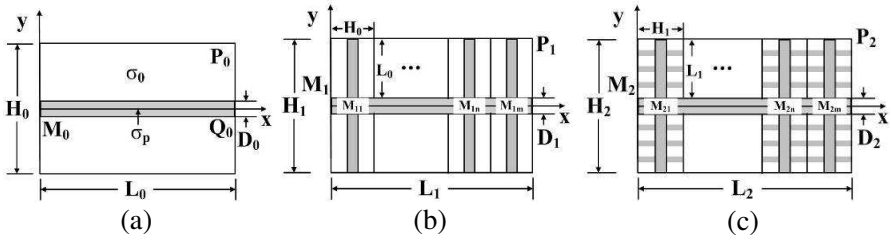

Figure 1. Construction of tree shaped network: (a) the elemental cell; (b) the 1st order assembly; (c) the 2nd order assembly.

are the combination of the metal patches and narrow connections named bridges. The bridges can be selected from straight line, meander line, L bridge, S bridge, etc. [3]. Many researchers have analyzed the electromagnetic behavior of planar EBG structures when designed on a PCB [2–5]. Paper [2] gives a simple and efficient design procedure for planar EBG structures which is sized from the band-gap starting and ending frequencies. [4] introduces the art modeling methodology of EBG structure based on physics-based equivalent circuit model. The researches show that the patches and bridges form equivalent inductor and capacitor (LC) networks. Steep noise suppression behavior results in the need for longer bridges and more slits in planar EBG structure, so voltage drop of the power plane becomes critical. Power distribution network (PDN) is needed to transfer currents to each unit cell in power plane for lower voltage drop and becomes one of the major concern in high speed circuits or mixed-signal systems in recent years [13, 14].

Bejan et al. (1997–2000) developed "constructal theory" [15–21] by optimizing the access between one point and many points situated in an area. Constructal networks represent a new trend in the optimization and miniaturization of heat transfer devices [18], mass exchangers [19], chemical reactors [20], fuel cells [21] and even economics [16]. Constructal theory provides a shortcut toward lower resistance. Its solution is the simplest structure that (i) is a tree shaped network, (ii) is deterministic, and (iii) is hierarchical.

In this paper, a constructal tree shaped network is constructed, and an EBG structure power plane with 2nd order tree shaped network is developed. Compared with conventional EBG structure plane, it has multi-functions of low voltage drop, current equidistribution, compactness and effective noise isolation.

The rest of the paper is organized as follows. Section 2 constructs tree shaped network. Section 3 is PCB power plane with this constructal network design example. Conclusion is given in Section 4.

2. CONSTRUCTAL TREE SHAPED NETWORK

2.1. Description of the Constructal Tree Shaped Network

Constructal theory was originally proposed to solve the "area to point" heat conduction problem [15] in engineering devices, which can be described as how to determine the optimal distribution of high conductivity material through the given area such that the heat generated at every point was transferred most effectively to its boundary. This solution was based on the rectangular elemental area as shown in Figure 1(a). Heat generated at every point of blank place with low thermal conductivity in Figure 1 was collected by the high thermal conductivity path. The maximum temperature difference was minimized, and the corresponding optimal elemental shape was obtained. Then a relatively larger heat generating area was designed and optimized by introducing a new link of high conductivity material. N_1 optimized elemental blocks were assembled on the upper and lower sides of the new link. There exists an optimal N_1 corresponding to the minimization of maximum temperature difference of the assembled area (the first assembly). The sequence of assembly of previously optimized flow surfaces into a larger flow surface and geometric optimization of the larger surface is continued until the required flow surface is obtained (second, third, ..., nth assembly). In this paper, the flow is direct current in power plane for high speed integrated circuit. The power plane is designed by constructal theory for optimized direct current distribution. Current distributing problem is another "area to point" conducting problem.

We assumed that the EBG structures in power plane have uniform electrical conductivity σ_0 and cover the blanks in Figure 1. They sink current uniformly (current density J) which is fed through a metal (high conductivity σ_p, $\sigma_p \gg \sigma_0$) network (the gray paths in Figure 1).

Figure 1(a) is called "elemental cell" or "0 order structure". Figure 1(b) is the "1st order assembly" assembled by N_1 "elemental cells". Figure 1(c) is the "2nd order assembly" assembled by N_2 "1st order assemblies". Constructing the given area in a sequence of building blocks from the smallest size toward larger sizes hierarchically can develop "ith order assembly" assembled by N_i "$(i-1)$th order assembly". The network is fed by outside DC connected at the point M. The areas of σ_p paths (A_{p0}, A_{p1}, etc.), the blocks areas (A_0, A_1, etc. are given, $A_{pi} \ll A_i$). $\phi = A_{pi}/A_i$ is defined. The degrees of freedom are width/length ratios H_0/L_0, H_1/L_1 etc., H_i/L_i, σ_p paths ratios D_1/D_0, D_2/D_1, etc., D_{i+1}/D_i. The object is to find the optimal configuration H_i/L_i, D_{i+1}/D_i and N_i such that the resistance is minimized. For simplicity, we made the thickness of each σ_p path

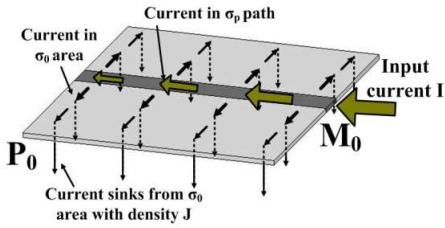

Figure 2. Current in elemental area.

constant.

2.2. Optimization of the "Elemental Cell"

In Figure 1(a), the current in the "elemental cell" is firstly delivered by the metal path, from which the current source located at the center is connected, then distributed to σ_0 area uniformly (shown in Figure 2). Assume that the "elemental cell" has one dimensional (y direction) current conduction in the σ_0 area. The σ_0 area uniformly consumes current density J. The boundary of the "elemental cell" is electric insulation except the source point M_0 (0, 0).

Homogenous Neumann conditions are given on all sides of the rectangle. In the region that sinks current, according to Laplace-Poisson equation for electrical potential V_0 and the boundary condition:

$$\begin{cases} \partial^2 V_0/\partial x^2 + \partial^2 V_0/\partial y^2 = J/\sigma_0 \\ \partial V_0/\partial y|_{y=H_0/2} = 0, \quad V_0(x,0) = V_{p0}(x) \end{cases} \tag{1}$$

where H_0 is the height of elemental cell, $V(x, y)$ the voltage of any point and $V_{p0}(x)$ the voltage along the x axis. We can obtain the voltage of any point

$$V(x,y) = V_{p0}(x) - \frac{1}{2}\frac{Jy^2}{\sigma_0} \tag{2}$$

The conduction problem along the x axis is:

$$\begin{cases} \sigma_p D_0 d^2 V_{p0}/dx^2 + JH_0 = 0 \\ dV_{p0}/dx|_{x=L_0} = 0, \quad V_{p0}(0) = V_0(0,0) \end{cases} \tag{3}$$

where D_0 and L_0 are the cross-section of its high conductivity path and the length of elemental cell, respectively. The voltage along the x axis is:

$$V_{p0}(x) = V(0,0) - \frac{JH_0L_0}{2\sigma_p D_0}x \tag{4}$$

Obviously, the voltage drop ΔV_0 is between the farthest corner P_0 (L_0, $H_0/2$) and current source point M_0 (0, 0). According to Equations (2) and (4), the voltage drop and resistance are:

$$\Delta V_0 = V(0,0) - V\left(L_0, \frac{H_0}{2}\right) = \frac{JH_0^2}{8\sigma_0} + \frac{JH_0L_0^2}{2\sigma_p D_0} \tag{5}$$

$$R_0 = \frac{\Delta V_0}{JA_0} = \frac{1}{8\sigma_0}\frac{H_0}{L_0} + \frac{1}{2\sigma_p\phi_0}\frac{L_0}{H_0} \tag{6}$$

where, $\phi_0 = A_{p0}/A_0$, J is the current density. Taking the derivative of Equation (6) with respect to H_0/L_0 and setting it to zero, the minimized resistance R_0 and corresponding H_0/L_0 can be obtained:

$$\begin{cases} (R_0)_{\min} = 0.5\left(\sigma_0\sigma_p\phi_0\right)^{-0.5} \\ (H_0/L_0)_{opt} = 2\left[\sigma_0/\left(\sigma_p\phi_0\right)\right]^{0.5} \end{cases} \tag{7}$$

And the minimized voltage drop is:

$$\Delta V_{0,\min} = \frac{JH_0^2}{8\sigma_0} + \frac{JH_0L_0^2}{2\sigma_p D_0} = \frac{JH_0^2}{8\sigma_0} + \frac{JL_0^2}{2\sigma_p\phi_0} = \frac{JH_0^2}{4\sigma_0} \tag{8}$$

which means that when the shape of this plane is determined according to Equation (7), the voltage drop of this plane is minimal.

2.3. Constructing the "1st Order Assembly" and "2nd Order Assembly"

The "1st order assembly" is assembled by N_1 optimal "elemental cells". N_1 is assumed to be a large number. The way to connect the elemental cells is shown in Figure 1(b). N_1 "elemental cells" are laid out on both sides of a new metal path D_1, such that the elemental direct current (DC) is conducted by the new path. The outer boundary of this area is electric insulation except the source point M_1 (0, 0). The voltage drop between point M_1 (0, 0) and M_{1m} is V_{p1}, which is approximately equal to the one between M_1 and N_1. The conduction problem along the x axis is:

$$\begin{cases} \sigma_p D_0 d^2V_{p1}/dx^2 + JH_1 = 0 \\ dV_{p1}/dx|_{x=L_1} = 0, \quad V_{p1}(0) = V_1(0,0) \end{cases} \tag{9}$$

where V_{p1} is the voltage along the x axis, and V_{p1} is:

$$\Delta V_{p1} = \frac{JH_1L_1^2}{2\sigma_p D_1} \tag{10}$$

The voltage drop between M_{1m} and P_1 is $V_{0,\min}$. In a similar way, the voltage drop and resistance of this structure can be obtained:

$$\Delta V_1 = \Delta V_{0,\min} + \Delta V_{p1} = \frac{JH_0^2}{4\sigma_0} + \frac{JH_1L_1^2}{2\sigma_p D_1} \tag{11}$$

$$R_1 = \frac{1}{4\sigma_p\phi_0}\frac{H_1}{L_1} + \frac{1}{2\sigma_p(\phi_1-\phi_0)}\frac{L_1}{H_1} \tag{12}$$

In Equation (12) $\phi_1 = A_{p1}/A_1$, $A_1 = H_1/L_1$, and the area of all the metal paths is:

$$A_{p1} = D_1L_1 + N_1D_0L_0 \tag{13}$$

By the same method as used in constructing elemental cell, when $\phi_1 = 2\phi_0$, the optimal resistance and voltage drop are obtained.

$$\begin{cases} \Delta V_{1,\min} = 0.5JH_0^2/\sigma_0 \\ (R_1)_{\min} = \left(\sqrt{2}/2\right)/(\sigma_p\phi_0) \end{cases} \tag{14}$$

The corresponding optimal geometry dimensions are:

$$\begin{cases} (D_1/D_0)_{opt} = 1/\sqrt{2}\,(\sigma_p/\sigma_0\phi_0)^{1/2} \\ (H_1/L_1)_{opt} = \sqrt{2} \\ (N_1)_{opt} = 2L_1/H_0 = (\sigma_p/\sigma_0\phi_1)^{1/2} \end{cases} \tag{15}$$

The constructal 1st order assembly is shown in Figure 3(a) according to results (14) and (15).

Figure 1(c) shows a 2nd order assembly, which is composed of a large number (N_2) of 1st order assemblies aligned on both sides of a path of width D_2. Following the steps from Equations (9) to (15), we can easily obtain that $N_2 = 2\sqrt{2} \approx 2.8$. Therefore, the optimal number of optimized first order assembly constructs making the second order assembly construct should be either 2 or 4.

When $N_{2,opt} = 2$, this value is small. For reducing area of metal paths, the D_2 path need not extend all the way across the large square. The construct is shown in Figure 3(b). The constructing method must be different. The voltage drop in Figure 3(b) is the sum of $V_{p2,N_2=2}$ and $V_{1,\min}$. $V_{p2,N_2=2}$ is the voltage drop between points M_2 and M_{21} along the path. The voltage drop and resistance of second assembly in Figure 3(b) are:

$$\Delta V_{2,N_2=2} = \Delta V_{1,\min} + \Delta V_{p2,N_2=2} = \frac{JH_0^2}{2\sigma_0} + \frac{JH_2L_2^2}{2\sigma D_2} \tag{16}$$

$$\begin{aligned} R_{2,N_2=2} &= \Delta V_{2,N_2=2}/(JA_2) \\ &= \sqrt{2}/2 \times (\sigma_p\phi_1)^{-1} + \left(4\sqrt{2}\sigma_p\,(\phi_2-\phi_1)\right)^{-1} \end{aligned} \tag{17}$$

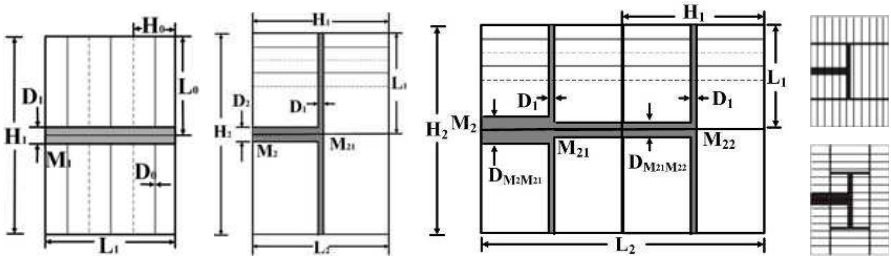

Figure 3. (a) The optimal 1st assembly. (b) The 2nd assembly when $N_{2,opt} = 2$. (c) The 2nd assembly when $N_{2,opt} = 4$. (d) The optimal 3rd and 4th order assemblies.

When $\phi_1 = 2/3\phi_2$, the minimized voltage drop and resistance will be obtained:

$$\begin{cases} \Delta V_{2,N_2=2,\min} = 0.75JH_0^2/\sigma_0 \\ R_{2,N_2=2,\min} = 9\sqrt{2}/8 \cdot (\sigma_p\phi_2)^{-1} = 1.5910/(\sigma_p\phi_2) \end{cases} \tag{18}$$

The corresponding geometric dimensions are:

$$\begin{cases} H_2/L_2 = \sqrt{2} \\ D_2/D_1 = 2\sqrt{2} \end{cases} \tag{19}$$

When $N_{2,opt} = 4$, the construct is shown in Figure 3(c), and it is reasonable to use the method based on discrete variable cross-section conducting path in which the conducting path cross-section along M_2M_{21} is different from $M_{21}M_{22}$. The voltage drop between M_2 and M_{22} is:

$$\Delta V_{M_2M_{22}} = \Delta V_{M_2M_{21}} + \Delta V_{M_{21}M_{22}} = \frac{JH_2L_2^2}{4\sigma_p\lambda D_{M_{21}M_{22}}} + \frac{JH_2L_2^2}{4\sigma_p D_{M_{21}M_{22}}} \tag{20}$$

where $\lambda = D_{M_2M_{21}}/D_{M_{21}M_{22}}$. For $\phi_2 - \phi_1 = (D_{M_2M_{21}}H_1/2 + D_{M_{21}M_{22}}H_1)/(N_2A_1)$. The minimized $\Delta V_{M_2M_{22}}$ is obtained when $\lambda = \sqrt{2}$.

$$\Delta V_{M_2M_{22},\min} = \frac{\left(3\sqrt{2}+4\right)}{16}\frac{JH_2L_2}{\sigma_p\left(\phi_2-\phi_1\right)} \tag{21}$$

Then the voltage drop and resistance are:

$$\Delta V_{2,N_2=4} = \frac{\sqrt{2}}{4}\frac{JH_2L_2}{\sigma_p\phi_1} + \frac{\left(3\sqrt{2}+4\right)}{16}\frac{JH_2L_2}{\sigma_p(\phi_2-\phi_1)} \tag{22}$$

$$R_{2,N_2=4} = \sqrt{2}/\left(4\sigma_p\phi_1\right) + \left(3\sqrt{2}+4\right)/\left[16\sigma_p\left(\phi_2-\phi_1\right)\right] \tag{23}$$

Taking the derivative of Equation (23) with respect to and setting it to zero yields that when $\phi_1 = 2(3-\sqrt{2})/7 \cdot \phi_2$:

$$R_{2,N_2=4,\min} = 1.7223/(\sigma_p \phi_2) \tag{24}$$

Comparing the optimization results of $N_{2,opt} = 2$ in Equation (18) with those of $N_{2,opt} = 4$, one can find that the second assembly achieves its minimum resistance at $N_{2,opt} = 2$.

2.4. The Data for the "*i*th Order Assemblies"

Other structures ("*i*th order assembly", $i > 2$) can be calculated with the same method as above. The optimal geometric dimensions of each order are:

$$\begin{cases} D_i = 2^{i-1/2}\sqrt{\sigma_p/\sigma_0\phi_0}D_0 \\ H_i = 2^{(i-1)/2}\sqrt{\sigma_p/\sigma_0\phi_0}H_0 \\ L_i = 2^{i/2-1}\sqrt{\sigma_p/\sigma_0\phi_0}H_0 \\ \phi_i = \phi_{i-1} + 2^{i/2-1}\phi_0 \end{cases} \quad (i \geq 2) \tag{25}$$

Obviously, $D_{i+1}/D_1 = 2$ and $H_i/L_i = \sqrt{2}$ when $i > 2$. In accordance with Equations (8), (14) and (18), ΔV_i has a factor JH_0^2/σ_0, and we define that:

$$\Delta V_i = v_i JH_0^2/\sigma_0 \tag{26}$$

The minimized voltage drop and resistance can be obtained by a recursion formula:

$$\begin{cases} \Delta V_{i,\min} = v_{i-1}JH_0^2/\sigma_0 + 0.5JH_iL_i^2/(\sigma_p D_i) \\ R_{i,\min} = v_i 2^{3/2-i}(\sigma_p\phi_0)^{-1} \end{cases} \tag{27}$$

The optimized "3rd order assembly" and "4th order assembly" are shown in Figure 3(c). The minimized voltage drops, resistances, and the corresponding optimal geometric parameters for 0 to the 3rd constructs are shown in Table 1. The optimal resistance R_i and voltage

Table 1. The voltage drops, resistances, and the optimal configuration parameters for the *i*th assemblies.

i	N_i	H_i/L_i	D_i/D_{i-1}	ΔV_i	R_i	ϕ_1/ϕ_0
0	-	$\sqrt{4\sigma_0/(\phi_0\sigma_p)}$	-	$0.250JH_0^2/\sigma_0$	$0.500/\sqrt{\sigma_p\sigma_0\phi_0}$	1
1	$\sqrt{\phi_1\sigma_p/\sigma_0}$	$\sqrt{2}$	$\sqrt{\phi_0\sigma_p/\sigma_0}$	$0.500JH_0^2/\sigma_0$	$0.707/(\sigma_p\phi_0)$	2
2	2	$\sqrt{2}$	$2\sqrt{2}$	$0.750JH_0^2/\sigma_0$	$0.530/(\sigma_p\phi_0)$	3
3	2	$\sqrt{2}$	2	$1.104JH_0^2/\sigma_0$	$0.390/(\sigma_p\phi_0)$	4.4142
4	2	$\sqrt{2}$	2	$1.604JH_0^2/\sigma_0$	$0.284/(\sigma_p\phi_0)$	6.4142

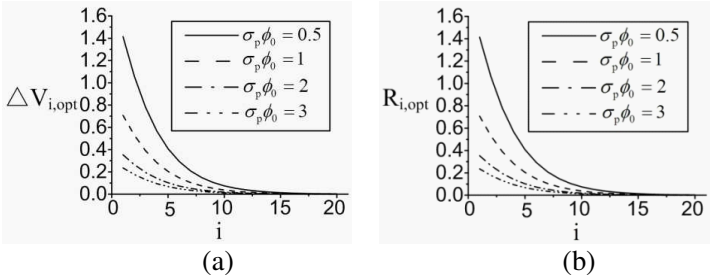

Figure 4. (a) The minimized voltage drop of "ith order assembly" when input current is 1 A. (b) The minimized resistance of "ith order assembly".

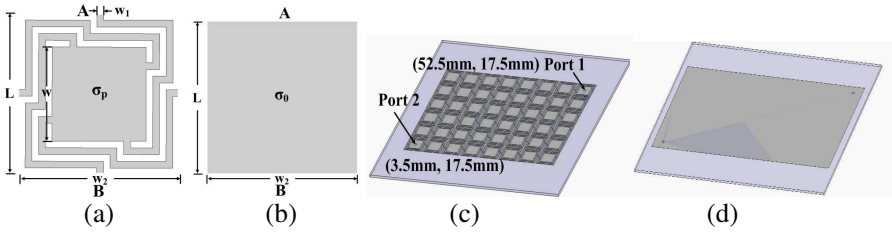

Figure 5. (a) EBG structure unit. (b) The solid patch with conductivity σ_0. (c) EBG power plane without network. (d) The referent solid plane.

drop as function of the i for the "ith order assemblies" are shown in Figure 4.

Important conclusions are made: the ith assembly is assembled by two $(i-1)$th assemblies for optimal resistance; the optimal aspect ratios $(H/L)_{opt} = \sqrt{2}$; the resistance decreases when i increases. Also from the figures, we know that $\sigma_p\phi_0$ is a key factor. When $i \geqslant 1$, the larger is $\sigma_p\phi_0$, the smaller are the resistance and voltage drop.

3. TREE SHAPED NETWORK DESIGN EXAMPLE FOR PCB POWER PLANE

3.1. Description of PCB Power Plane

The objective in this section is to form an EBG power plane based on the 2nd order assembly network. Figure 5(a) is the EBG structure unit. Figure 5(c) is the EBG power plane (6×8 units) without network, and Figure 5(d) is a referent solid 2 sided power plane. The EBG unit in

Figure 5(a) with high conductivity σ_p can be regarded as a solid patch (shown in Figure 5(b)) with the same size and equivalent conductivity σ_p. The resistance between A and B in Figure5(a) is the same as the one between A and B in Figure 5(b). We can obtain the ratio between metal conductivity σ_p and equivalent conductivity σ_0:

$$\sigma_p/\sigma_0 = w_2/w_1 \times 2l/L \tag{28}$$

where l is length of the bridges.

In Figure 5(a), $L = 7\,\text{mm}$, $w = 4.2\,\text{mm}$, $w_1 = 0.3\,\text{mm}$, $w_2 = 7\,\text{mm}$, $l = 14.2\,\text{mm}$. According to Equation (17), $\sigma_p/\sigma_0 \approx 90$. Figure 6(a) is the 2nd order tree shaped network. $\phi_0 = 0.065$. According to Equation (13), size of the 2nd order assembly in Figure 6(a) is $44.1\,\text{mm} \times 60.6\,\text{mm}$, $D_0 = 0.87\,\text{mm}$, $D_1 = 2.1\,\text{mm}$ and $D_2 = 5.9\,\text{mm}$. Figure 6(c) is the designed EBG power plane by assembling the EBG

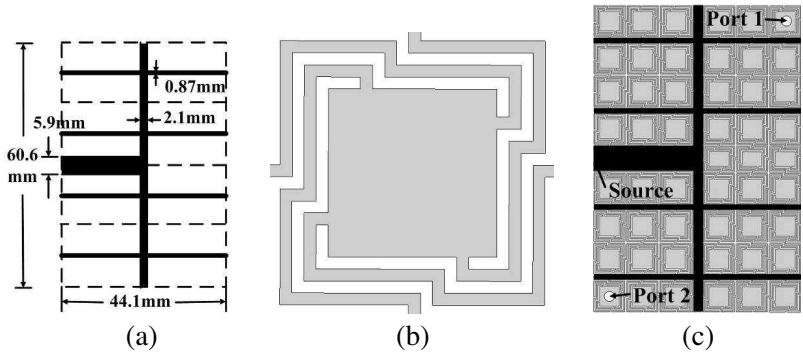

Figure 6. (a) The 2nd order tree shaped network. (b) The EBG unit. (c) The 2nd order plane.

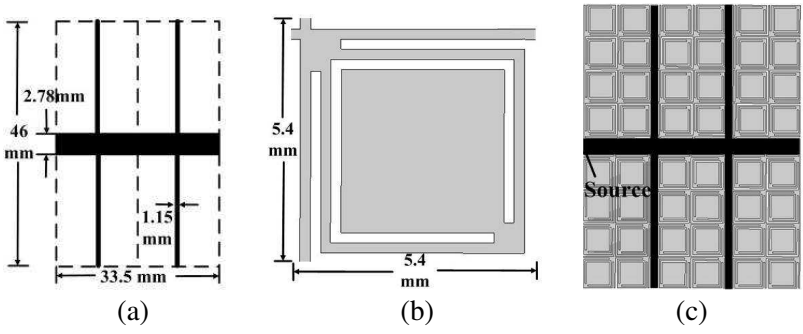

Figure 7. Another example of EGB power plane base on the 1st order tree shaped network. (a) The 1st order tree network. (b) The EBG unit designed in [22]. (c) The 1st order plane.

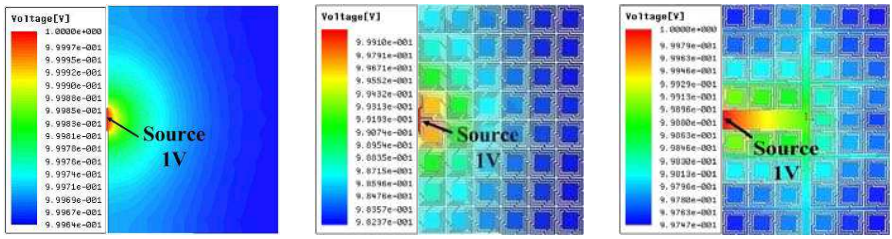

(a) (b) (c)

Figure 8. The voltage drops of (a) the referent plane; (a) the EBG power plane; (b) the 2nd order plane.

Table 2. The voltage distribution and resistance of the referent plane, EBG power plane and designed plane with the 2nd order tree shaped network.

Plane	**Solid referent plane in Figure 5(d)**	**EBG power plane in Figure 5(c)**	**The 2nd order plane in Figure 6(c)**
Voltage (V)	1 to 0.9994	1 to 0.9824	1 to 0.9975
Resistance (Ohm)	1.8653×10^{-4}	3.1788×10^{-3}	1.5150×10^{-3}

units to the network in Figure 6(a). The plane is applied on a two layer FR-4 PCB structure with thickness 0.8 mm and dielectric constant 4.4.

This optimization algorithm can also be used to design networks for other types of planar EBG structures. Figure 7 shows another example where the planar EBG structures designed in [22] are used. This design is based on the 1st order assembly. According to the analysis before, the optimal geometry parameters are shown in Figure 7(a).

3.2. Voltage Drop, Resistance and Equidistribution Property

Figure 8 shows the voltage distribution for the designed plane in Figure 6, solid referent plane and EBG power plane with excitations (total sink current 1 A and voltage 1 V) simulated by Ansoft Maxwell 3D. The current distribution (shown in Figure 9) and the resistances for these planes with excitations (total sink current 1 A and voltage 1 V) are simulated by Ansoft Q3D. The current sinks from the center of each EBG unit. The simulated voltage and resistance results are in Table 2.

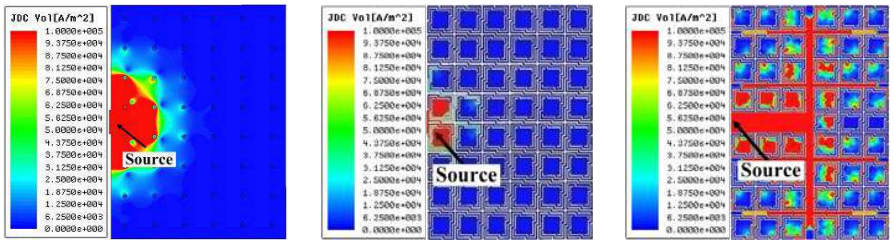

(a) (b) (c)

Figure 9. Current distribution of (a) referent plane; (c) the EBG power plane; (b) the 2nd order plane.

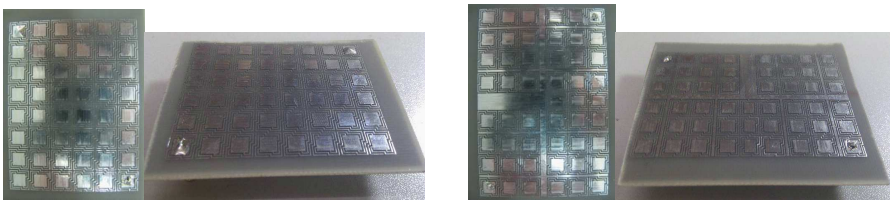

(a) (b)

Figure 10. The power plane of (a) the EBG power plane; (b) the 2nd order plane.

The voltage drops and resistances by the designed plane are lower than those of referent plane, which means that the constructal tree shaped network can provide EBG power plane with low voltage drop performance.

In Figures 9(a) and (b), current is distributed only around the source. In Figure 9(c), the 2nd order tree shaped network transmits current to each EBG unit in the power plane, i.e., current equidistribution property is obtained from the constructed tree shaped plane, though the resistance of the 2nd order plane is larger than the solid referent plane owing to the long bridges and slits.

3.3. Noise Suppression

Figure 10(a) is the prototype of the experiment for the EBG power plane, and Fig. 10(b) is the one for the 2nd order plane. Ansoft high frequency structure simulator (HFSS) is used to simulate transmission coefficient S_{21}. Agilent network analyzer N5230A is used to measure the transmission coefficient. Locations for the exciting and receiving ports are shown in Figures 5 and 6. The simulated and measured S_{21} for the referent plane, EBG power plane and the 2nd order plane with

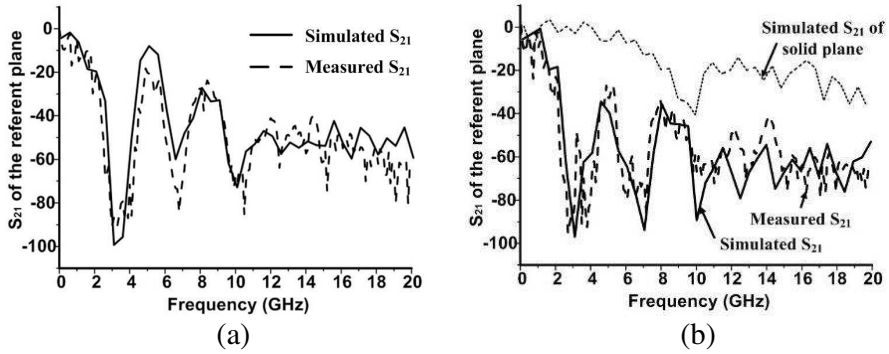

Figure 11. (a) The simulated and measured S_{21} of the EBG power plane. (b) The simulated and measured S_{21} of the 2nd order plane and simulated S_{21} of solid referent plane.

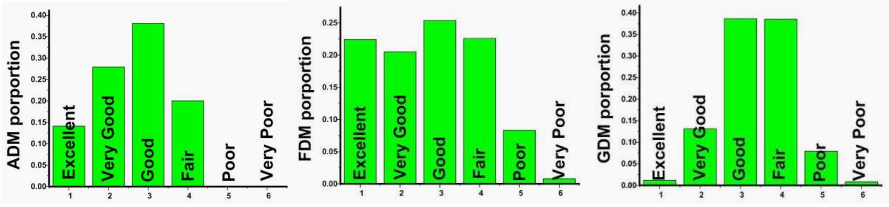

Figure 12. FSV results for comparison in Figure 11(b). (a) ADM; (b) FDM and (c) GDM.

solid ground planes are shown in Figure 11. The mental paths of the tree shaped network do not apparently affect the noise suppression of the plane. The band gap defined as the domain where the S_{21} is lower than -20 dB begins from about 2 GHz. However, though this designed plane would most likely degrade the high-speed signals passing over the EBG patterns because of the discontinuities of the etched power plane, this plane has a limitation in terms of the expansion of the lower band-gap frequency due to the physical size of the EBG units. An EBG-patterned board with decoupling capacitors can be a means of both suppressing noise propagation from extremely low frequencies and minimizing the effects of the discontinuous plane [23].

Figure 12 reports the values of amplitude difference measure (ADM), feature difference measure (FDM) and global difference measure (GDM) evaluated by using the feature selective validation (FSV) technique [24–26] according to the recent IEEE Standard P1597.1 [24] for a significant quantification of the comparison between the measured and simulated values in Figure 11(b).

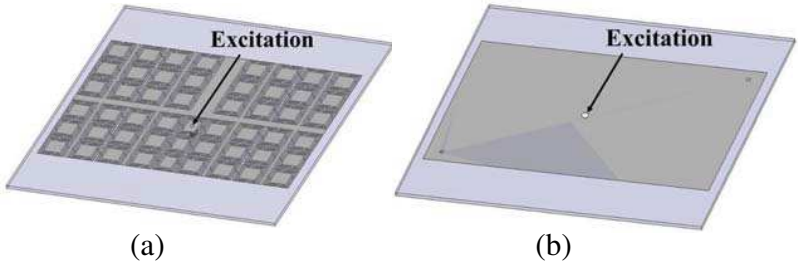

Figure 13. The location of the excitation of (a) the designed plane; (b) the referent solid plane.

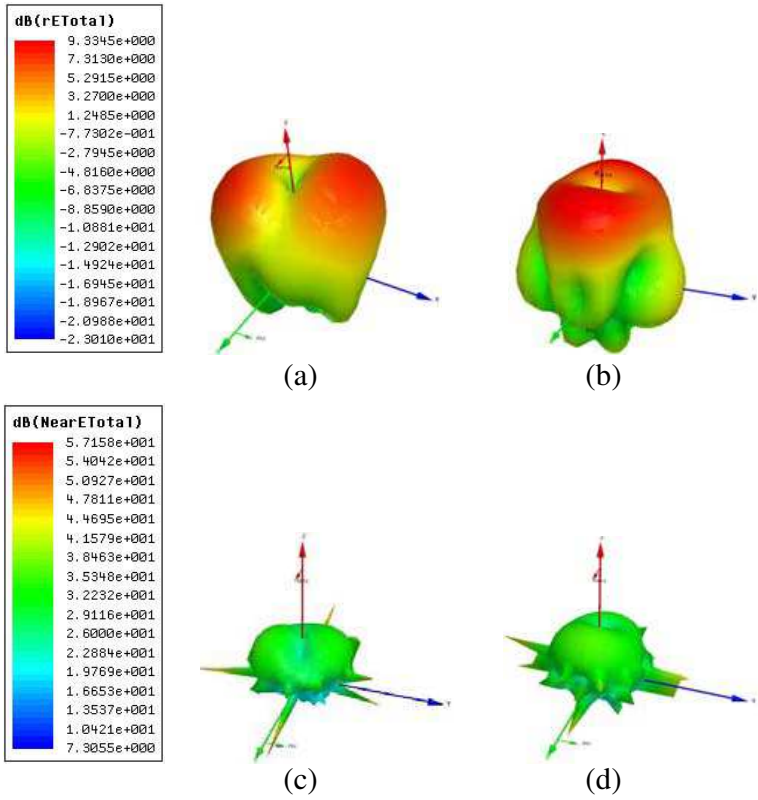

Figure 14. Far field directional diagrams of (a) designed plane and (b) referent plane. Near field directional diagrams of (c) designed plane and (b) referent plane.

Table 3. The electromagnetic radiation quantities (dB) of far field and near field of these planes.

Plane	The 2nd order plane in Figure 13(a)	The referent solid plane in Figure 13(b)
Far field	About −12.90 to 7.310	About −12.23 to 9.3345
Near field	About 7.30 to 57.15	About 7.30 to 54.04

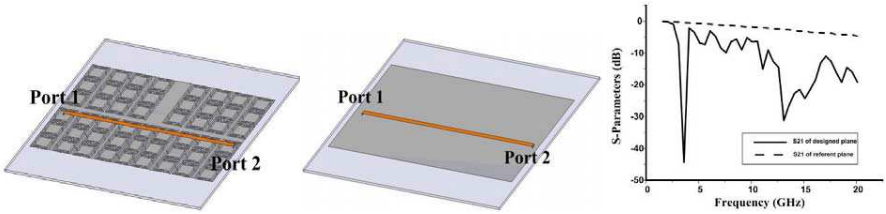

(a) (b) (c)

Figure 15. Three-layer board with transmission line of (a) designed plane and (b) referent solid plane; (c) S_{21} of the two planes.

3.4. Electromagnetic Radiation and Signal Integrity Analysis

Although the proposed power plane shows ultra-wideband suppression of SSN, the presence of slits and bridges might enhance the electromagnetic radiation and degrade the quality of signals propagating on traces. An exciting port is located at point (0 mm, 6.3 mm) in the designed plane as a noise excitation, shown in Figure 13(a). A referent solid plane in Figure 13(b) is used for comparison. The directivity diagrams of near field and far field are shown in Figure 14. The quantities of electromagnetic radiation are shown in Table 3. The slits and bridges in designed plane hardly affect the quantity of radiation.

For analyzing signal integrity, a three-layer board is designed shown in Figure 15(a). A single-ended signaling approach is adopted on the top layer of this board. Figure 15(b) shows a solid referent plane for comparison. The traces are designed with impedance of 50 Ohm. The width of the lines is 1.5 mm. Ports 1, 2 are located at both ends of the lines. The S-parameters of these lines are shown in Figure 15(c). The S-parameters of designed plane are worse than

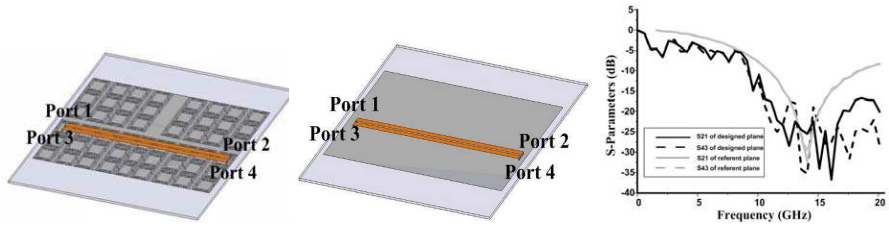

(a) (b) (c)

Figure 16. Three-layer board with differential transmission lines of (a) designed plane and (b) referent solid plane; (c) S_{21} and S_{43} of the two planes.

those of solid plane for the slits and bridges. In order to improve the signal quality, a differential signaling couple approach is adopted. Figures 16(a) and (b) show a three-layer EBG board and referent solid board with differential transmission lines, respectively. The traces are designed with a differential impedance of 50 Ohm. The width of the lines is 1.5 mm, and the spacing between the two lines is 0.5 mm. The S-parameters are shown in Figure 16(c). It can be seen that the S-parameters of the designed board are not worse a lot than those of the solid plane. The signal quality is improved.

4. CONCLUSION

In this paper, a tree shaped network is designed based on constructal theory. The optimal configuration ratio, optimal assembly number and network dimensions are obtained for optimal voltage drop and resistance. A plane is designed based on the designed tree shaped networks, and a tradition EBG power plane without tree shaped network is used for reference. The current densities for the designed plane is more uniform than that for referent plane. The voltage drop and resistance for the designed plane are lower. In the meantime, the designed plane has proved its wideband noise isolation performance. That is, the designed power plane has multi-functions of equidistribution, low voltage drop, current compactness and noise isolation while maintaining a relatively simple design of geometry.

ACKNOWLEDGMENT

This project is supported by Research Fund for the Doctoral Program of Higher Education of China (20090172120009) and National Science Foundation of China (61071056).

REFERENCES

1. Eudes, T., B. Ravelo, and A. Louis, "Transient response characterization of the high-speed interconnection RLCG-model for the signal integrity analysis," *Progress In Electromagnetics Research*, Vol. 112, 183–197, 2011.
2. Raimondo, L., F. de Paulis, and A. Orlandi, "A simple and efficient design procedure for planar electromagnetic band-gap structures on printed circuit boards," *IEEE Transactions on Electromagnetic Compatibility*, Vol. 52, No. 3, Nov. 2010.
3. He, Y., L. Li, C. H. Liang, Q. H. Liu, L. Li, and H. B. Wen, "Leafy EBG structures for ultra-wideband SSN suppression in power/ground plane pairs," *Electronics Letters*, Vol. 46, No. 11, 768–769, May 27, 2010.
4. Wu, T. L., J. Fan, F. de Paulis, C. D. Wang, A. Ciccomancini Scogna, and A. Orlandi, "Mitigation of noise coupling in multilayer high-speed PCB: State of the art modeling methodology and EBG technology," *Journal of Institute of Electronics, Information and Communication Engineers (IECE)*, Vol. E93-B, No. 7, Jul. 2010.
5. De Paulis, F., L. Raimondo, S. Connor, B. Archambeault, and A. Orlandi, "Design of a common mode filter by using planar electromagnetic bandgap structures," *IEEE Transactions on Advanced Packaging*, Vol. 33, No. 4, 994–1002, Nov. 2010.
6. Xu, H.-J., Y.-H. Zhang, and Y. Fan, "Analysis of the connection between K connector and microstrip with electromagnetic bandgap (EBG) structures," *Progress In Electromagnetics Research*, Vol. 73, 239–247, 2007.
7. Moghadasi, S. M., A. R. Attari, and M. M. Mirsalehi, "Compact and wideband 1-D mushroom-like EBG filters," *Progress In Electromagnetics Research*, Vol. 83, 323–333, 2008.
8. Wang, X., M. Zhang, and S.-J. Wang, "Practicability analysis and application of PBG structures on cylindrical conformal microstrip antenna and array," *Progress In Electromagnetics Research*, Vol. 115, 495–507, 2011.
9. Kim, S.-H., T. T. Nguyen, and J.-H. Jang, "Reflection characteristics of 1-D EBG ground plane and its application to a planar dipole antenna," *Progress In Electromagnetics Research*, Vol. 120, 51–66, 2011.
10. Pirhadi, A., F. Keshmiri, M. Hakkak, and M. Tayarani, "Analysis and design of dual band high directive EBG resonator antenna using square loop FSS as superstrate layer," *Progress In*

Electromagnetics Research, Vol. 70, 1–20, 2007.

11. Wu, T.-L., Y.-H. Lin, T.-K. Wang, C.-C. Wang, and S.-T. Chen, "Electromagnetic bandgap power/ground planes for wideband suppression of ground bounce noise and radiated emission in high-speed circuits," *IEEE Transactions on Microwave Theory and Techniques*, Vol. 53, No. 9, 2935–2942, Sep. 2005.
12. Wang, T.-K., C.-Y. Hsieh, H.-H. Chuang, and T.-L. Wu, "Design and modeling of a stopband-enhanced EBG structure using ground surface perturbation lattice for power/ground noise suppression," *IEEE Transactions on Microwave Theory and Techniques*, Vol. 57, No. 8, 2047–2054, Aug. 2009.
13. Wu, T.-L., H.-H. Chuang, and T.-K. Wang, "Overview of power integrity solutions on package and PCB: Decoupling and EBG isolation," *IEEE Transactions on Electromagnetic Compatibility*, Vol. 52, No. 2, 346–356, May 2010.
14. Archambeault, B., C. Brench, and S. Connor, "Review of printed-circuit-board level EMI/EMC issues and tools," *IEEE Transactions on Electromagnetic Compatibility*, Vol. 52, No. 2, 455–461, May 2010.
15. Bejan, A., "Constructal theory: From thermodynamic and geometric optimization to predicting shape in nature," *Energy Conversion and Management*, Vol. 39, Nos. 16–18, 1705–1718, Nov. 1998.
16. Bejan, A., V. Badescu, and A. de Vos, "Constructal theory of economics," *Applied Energy*, Vol. 67, Nos. 1–2, 37–60, Sep. 2000.
17. Kang, D.-H., S. Lorente, and A. Bejan, "Constructal architecture for heating a stream by convection," *International Journal of Heat and Mass Transfer*, Vol. 53, Nos. 9–10, 2248–2255, Apr. 2010.
18. Da Silva, A. K. and A. Bejan, "Constructal multi-scale structure for maximal heat transfer density in natural convection," *International Journal of Heat and Fluid Flow*, Vol. 26, No. 1, 34–44, Feb. 2005.
19. Senn, S. M. and D. Poulikakos, "Laminar mixing, heat transfer and pressure drop in tree-like microchannel nets and their application for thermal management in polymer electrolyte fuel cells," *Journal of Power Sources*, Vol. 130, No. 1–2, 178–191, May 3, 2004.
20. Tescari, S., N. Mazet, and P. Neveu, "Constructal method to optimize solar thermochemical reactor design," *Solar Energy*, Vol. 84, No. 9, 1555–1566, Sep. 2010.

21. Sciacovelli, A. and V. Verda, "Entropy generation analysis in a monolithic-type solid oxide fuel cell (SOFC)," *Energy*, Vol. 34, No. 7, 850–865, Jul. 2009.
22. Farzan, S. M. D. and A. Sankar, "A new miniaturized planar electromagnetic bandgap (EBG) structure with dual slits," *12th Signal Propagation on Interconnects, SPI 2008*, 1–4, 2008.
23. Kwon, J.-H., S.-I. Kwak, and D.-U. Sim, "Localized EBG structure with DeCaps for ultra-wide suppression of power plane noise," *PIERS Proceedings*, 1474–1477, Marrakesh, Morocco, Mar. 20–23, 2011.
24. IEEE Standard P1597, Standard for Validation of Computational Electromagnetics Computer Modeling and Simulation — Part 1, 2, 2008.
25. Duffy, A. P., A. J. M. Martin, A. Orlandi, G. Antonini, T. M. Benson, and M. S. Woolfson, "Feature selective validation (FSV) for validation of computational electromagnetics (CEM). Part I — The FSV method," *IEEE Transactions on Electromagnetic Compatibility*, Vol. 48, No. 3, 449–459, Aug. 2006.
26. Orlandi, A., A. P. Duffy, B. Archambeault, G. Antonini, D. E. Coleby, and S. Connor, "Feature selective validation (FSV) for validation of computational electromagnetics (CEM). Part II — Assessment of FSV performance," *IEEE Transactions on Electromagnetic Compatibility*, Vol. 48, No. 3, 460–467, Aug. 2006.